Geochemistry Geophysics Geosystems G3
AN ELECTRONIC JOURNAL OF THE EARTH SCIENCES
Published by AGU and the Geochemical Society

Article
Volume 8, Number 5
11 May 2007
Q05006, doi:10.1029/2006GC001533
ISSN: 1525-2027

Evaluating hot spot–ridge interaction in the Atlantic from regional-scale seismic observations

James B. Gaherty
Lamont-Doherty Earth Observatory of Columbia University, 61 Route 9W, Palisades, New York 10964, USA (gaherty@ldeo.columbia.edu)

Robert A. Dunn
Department of Geology and Geophysics, University of Hawaii, Honolulu, Hawaii 96822, USA (dunnr@hawaii.edu)

[1] We probe variations in mantle temperature, composition, and fabric along hot spot–influenced sections of the Mid-Atlantic Ridge (MAR), using surface waves from nearby ridge earthquakes recorded on broadband island-based seismic stations. We invert frequency-dependent phase delays from these events to estimate one-dimensional mean shear velocity and radial shear anisotropy profiles in the upper 200 km of the mantle within two seafloor age intervals: 5–10 Ma and 15–20 Ma. Mean shear velocity profiles correlate with apparent hot spot flux: lithosphere formed near the low-flux Ascension hot spot is characterized by high mantle velocities, while the MAR near the higher-flux Azores hot spot has lower velocities. The impact of the high-flux Iceland hot spot on mantle velocities along the nearby MAR is strongly asymmetric: the lithospheric velocities near the Kolbeinsey ridge are moderately slow, while velocities near the Reykjanes ridge estimated in previous studies are much slower. Within each region the increase in shear velocity with age is consistent with a half-space cooling model, and the velocity variations observed between Ascension, the Azores, and Kolbeinsey are consistent with approximately ±75° potential-temperature variation among these sites. In comparison, the Reykjanes lithosphere is too slow to result purely from half-space cooling of a high-temperature mantle source. We speculate that the anomalously low shear velocities within the lithosphere produced at the Reykjanes ridge result from high asthenospheric temperatures of +50–75 K combined with ~12% (by volume) gabbro retained in the mantle due to the imbalance between high hot spot–influenced melt production and relatively inefficient melt extraction along the slow spreading Reykjanes. Radial shear anisotropy in the upper 150 km also indicates an apparent hot spot influence: mantle fabric near Ascension is quite weak, consistent with previous models of anisotropy produced by corner flow during slow seafloor spreading. The fabric near the Azores and the Kolbeinsey ridge is stronger, suggesting that the hot spot increases mantle deformation beyond that produced by slow seafloor spreading in these regions.

Components: 11,776 words, 9 figures.

Keywords: oceanic lithosphere; mid-ocean ridge; hot spots; surface waves.

Index Terms: 7245 Seismology: Mid-ocean ridges; 7218 Seismology: Lithosphere (1236); 7255 Seismology: Surface waves and free oscillations.

Received 17 November 2006; **Revised** 22 January 2007; **Accepted** 12 February 2007; **Published** 11 May 2007.

Gaherty, J. B., and R. A. Dunn (2007), Evaluating hot spot–ridge interaction in the Atlantic from regional-scale seismic observations, *Geochem. Geophys. Geosyst.*, *8*, Q05006, doi:10.1029/2006GC001533.

1. Introduction

[2] Along mid-ocean ridges, the dynamics of seafloor spreading are largely controlled by the interplay between two factors: the plate-spreading rate, and the composition and temperature of the mantle source. Spreading rate controls the rate at which mantle source material passively upwells beneath the ridge. Because spreading-rate varies slowly along ridges, the mantle flow structure induced by passive upwelling is largely two-dimensional (2-D), and to first-order, the resulting igneous crust is quite uniform in both composition and thickness [e.g., *White et al.*, 2001]. On the other hand, mantle composition and temperature control the degree to which melt-derived and thermally derived buoyancy drive upwelling [e.g., *Parmentier and Phipps Morgan*, 1990; *Jha et al.*, 1994]. Because the source characteristics may vary over many scales, they may be responsible for many of the variations observed in oceanic crustal structure [e.g., *Klein and Langmuir*, 1987].

[3] The influence of source heterogeneity on mid-ocean ridge dynamics can best be assessed at slow spreading rates, where source effects are exaggerated relative to spreading-rate effects. Active-source seismic surveys [*Tolstoy et al.*, 1993; *Hooft et al.*, 2000; *Dunn et al.*, 2005] have documented crustal-thickness variations on the Mid-Atlantic Ridge (MAR) at the segment scale that suggest strongly three-dimensional melt accumulation and focusing. At a larger scale, on- and near-axis hot spots are correlated with low-velocity (i.e., high-temperature) mantle source anomalies [e.g., *Montagner and Ritsema*, 2001; *Silveira and Stutzmann*, 2002; *Pilidou et al.*, 2004]. The relationship between these hot spot islands and deep-seated mantle plumes is debated [e.g., *Wolfe et al.*, 1997; *Bijwaard and Spakman*, 1999; *Foulger et al.*, 2000; *Montelli et al.*, 2004], but there is little question that at the depths associated with mantle melting and seafloor spreading, many hot spots have a substantial thermal signature [e.g., *Langmuir et al.*, 1993; *Allen et al.*, 2002; *Ito et al.*, 2003]. The impact of hot spot source anomalies on the spreading processes along the adjacent ridge systems can be seen in a variety of observables, including geochemical tracers [e.g., *Schilling*, 1973; *Schilling et al.*, 1999], gravity and topography [e.g., *Searle et al.*, 1998; *Escartin et al.*, 2001], and crustal thickness [e.g., *Smallwood et al.*, 1995]. The trends of these observables helps constrain the processes underlying the hot spot and its interaction with the spreading center, including the magnitude of the thermal anomaly, the magnitude and geometry of the material flux, and the mantle rheology [e.g., *Ito et al.*, 1996, 1999; *Yale and Phipps Morgan*, 1998; *Ito*, 2001].

[4] In this study, we investigate the thermal structure and mantle flow along several segments of the MAR that are influenced by a near-axis hot spot. These particularly strong source anomalies influence spreading processes hundreds of kilometers along the ridge axis, and as each plate moves off-axis, the thermal, compositional, and anisotropic impact of the hot spot influence should be retained within the lithosphere. This notion was exploited by *Gaherty* [2001], who utilized surface waves that traversed the length of the Reykjanes Ridge (RR) and the adjacent North Atlantic between the Charlie Gibbs Fracture Zone and broadband stations on Iceland (Figure 1) to construct age-dependent 1-D models of upper mantle shear velocity and radial anisotropy (a simplified parameterization of seismic anisotropy that contains a hexagonal symmetry axis normal to the Earth's surface). These models display a monotonic increase in mean shear velocity with age due to plate cooling (Figure 2a). At a given age, the mean velocities within lithosphere formed on the Reykjanes Ridge are lower than within Pacific lithosphere, implying higher temperatures beneath the Reykjanes than beneath the fast spreading East Pacific Rise. The resulting models also suggest strong radial anisotropy, with horizontal shear velocities (v_{SH}) slower than vertical shear velocities (v_{SV}) above ~100 km depth (Figure 2b). The anisotropy is small (unresolved) directly beneath the ridge, but it has a magnitude of ~5% in lithosphere older than ~5 Myr. This anisotropic fabric is unlike that found in other oceanic regions, which are characterized by $v_{SH} > v_{SV}$ throughout the upper mantle, presumably due to horizontal olivine fabric resulting from plate spreading (Figure 2b). On the basis of numerical models of fabric development during seafloor spreading [e.g., *Blackman and Kendall*, 2002], *Gaherty* [2001] interpreted the Reykjanes models as evidence for vertical olivine fabric developed by hot spot–fueled buoyant flow beneath the ridge. Alternative interpretations are possible [*Holtzman et al.*, 2003; *Delorey et al.*, 2007], but all conclude that a strong hot spot perturbation is needed to produce the anomalous structure.

[5] Here we extend this analysis elsewhere along the MAR. We focus on five ridge segments: the Kolbeinsey Ridge, stretching between Iceland and Jan Mayen, a possible hot spot to the north [*Schilling et al.*, 1999]; the MAR both north and

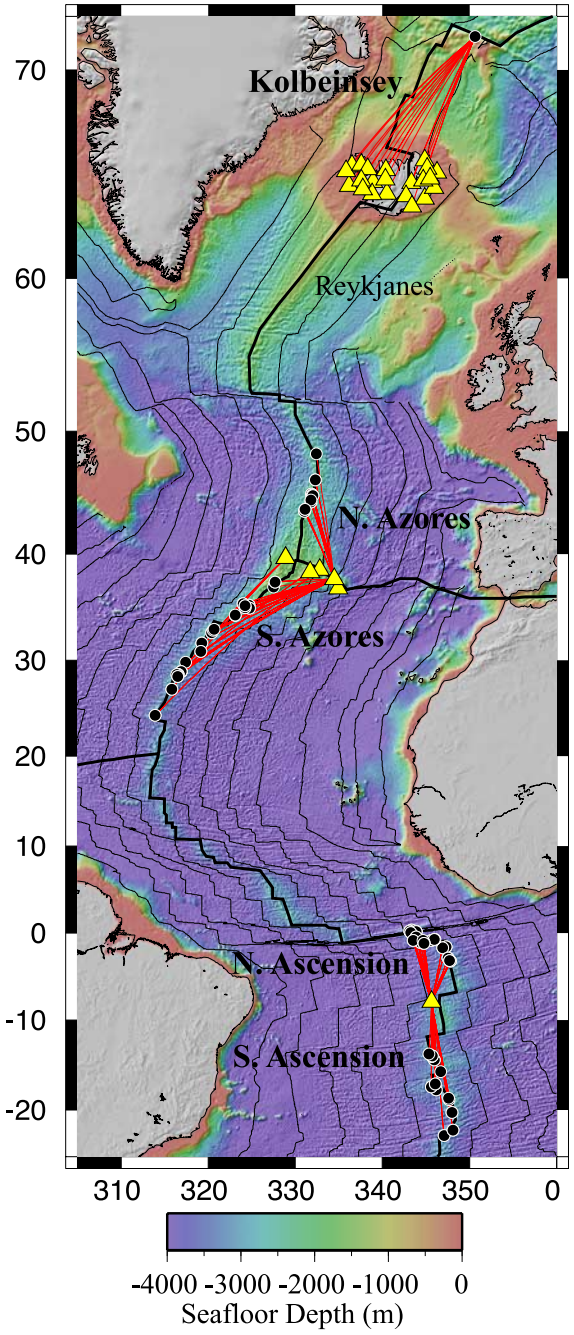

Figure 1. Predicted seafloor bathymetry map [*Smith and Sandwell*, 1997] of the Mid-Atlantic Ridge (MAR) study regions. Red lines represent surface-wave raypaths between MAR earthquakes (black circles) and island broadband seismic stations (yellow triangles). Seafloor age is contoured in 20 Ma intervals [*Mueller et al.*, 1993]. Shallow ridge crest bathymetry near Iceland suggests a strong hot spot influence; the hot spot influence near Azores is notable but significantly smaller than Iceland; and the MAR near Ascension is not notably shallower than the non–hot spot regions.

south of the Azores Islands archipelago; and the MAR both north and south of Ascension Island (Figure 1). All of these regions represent stretches of the MAR adjacent to near-ridge island-based seismic stations, and which may have been influenced by hot spot activity. In the cases of the Kolbeinsey ridge and the Azores ridge segments, this notion is supported by anomalously shallow bathymetry (Figure 1) and along-axis geochemical anomalies [*Dosso et al.*, 1999; *Goslin and Triatnord Scientific Party*, 1999; *Blichert-Toft et al.*, 2005]. Ascension Island does not have a broad depth anomaly, and it is debated as to whether it is produced by a hot spot or weak mantle compositional anomaly [e.g., *Brozena*, 1986; *Minshull et al.*, 2003], or whether it is the product of enhanced melt extraction at a ridge-transform intersection [e.g., *Klingelhofer et al.*, 2001]. Regardless, it is useful for this study, as it represents the apparent low-flux end of the ocean-island spectrum. In this context, Azores represents an intermediate flux hot spot, and Iceland a high flux hot spot.

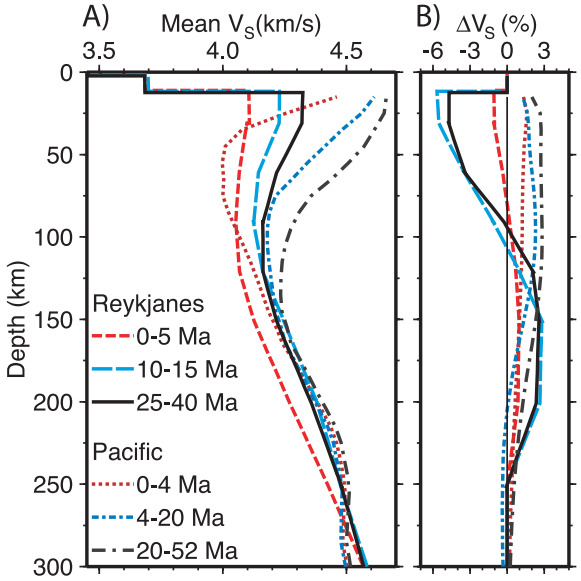

Figure 2. Mean shear wave velocity ($V_S = (V_{SH} + V_{SV})/2$) and shear anisotropy ($\Delta V_S = (V_{SH} - V_{SV})/V_S$) derived from radially anisotropic models of the Reykjanes ridge region, from *Gaherty* [2001], compared to comparable age models from the Pacific [*Nishimura and Forsyth*, 1988]. For the Reykjanes models, models represent mean seafloor ages of 0–5 Ma (red curves), 10–15 Ma (blue curves), and 25–40 Ma (black curves). The Pacific models generally represent a wider span of seafloor ages, but the mean ages coincide with that for the comparable Reykjanes model.

[6] We investigate upper-mantle structure beneath and adjacent to these stretches of the MAR using surface waves from regional events to estimate localized, age-dependent models of upper-mantle structure, including mean shear velocity and the degree of radial shear anisotropy. As in the Reykjanes study, the nearly ridge-parallel source-receiver paths provide good age resolution of the near-ridge lithospheric structure. The velocity structure of the lithosphere retains a record of ridge processes; the mean velocities reflect the mantle temperature and composition beneath the ridge, and anisotropy records flow characteristics. The resulting models can be directly compared to the Reykjanes models of *Gaherty* [2001], as well as published models from near the fast spreading EPR [*Nishimura and Forsyth*, 1988; *Gu et al.*, 2005]. The sampling of slow spreading lithosphere as a function of age is more limited than that found along the Reykjanes because of a much smaller number of receivers and/or sources, but we successfully quantify ridge structure on both sides of each hot spot, in one or more age intervals: 4–6 Ma, 5–10 Ma, and 15–20 Ma. By comparing the estimated isotropic and anisotropic shear velocity models for these regions, and placing them into context with the observations from the RR and EPR, we estimate the relative strength of the mantle source anomalies responsible for the hot spots, and the impact of these anomalies on flow structure beneath the ridge.

2. Surface-Wave Traveltimes

[7] We analyze traveltimes of surface waves from 58 moderate-sized earthquakes from the MAR that occurred between 5–20° epicentral distance of an island broadband seismic station (Figure 1). For events near Ascension, we used station ASCN of the Global Seismic Network (GSN) operated by the IRIS consortium [*Butler et al.*, 2004]. The Azores models are based primarily on GSN station CMLA, supplemented by recordings from the temporary MIDSEA experiment [*van der Lee et al.*, 2001]. The Kolbeinsey analysis is based on a single event recorded by the temporary HOTSPOT experiment [e.g., *Allen et al.*, 2002]. The seismograms were rotated into the receiver-source coordinate system and low-pass, zero-phase filtered with a corner at 45 mHz. All waveforms were inspected by comparing to full synthetics, and we rejected data with signal-to-noise (S/N) ratio less than approximately three. Synthetic seismograms were calculated for a spherically symmetric velocity model with a crustal thickness and water depth specified for each source-receiver path [*Laske et al.*, 2001], using a normal-mode technique. We assumed source locations and mechanisms obtained from the Global CMT catalog [e.g., *Ekström et al.*, 2005], and synthetics were convolved with the appropriate instrument responses and filtered like the data.

[8] We measured frequency-dependent traveltimes of these data using a cross-correlation analysis [*Gee and Jordan*, 1992; *Gaherty et al.*, 1996]. This methodology utilizes synthetic seismograms of a target wave group (in this case the fundamental-mode surface waves) to estimate phase delays of the observed arrival relative to the synthetic as a function of frequency. The synthetic wave group, called an "isolation filter", is cross-correlated with both the data and a complete synthetic seismogram (Figure 3a). The resulting cross-correlagrams are windowed and narrow-band (Gaussian) filtered at discrete frequency intervals (15, 20, 25, 30, 37, and 45 mHz), and the phase of each correlagram is estimated at each frequency. The phase delays are calculated by subtracting each synthetic/isolation-filter phase from the corresponding data/isolation-filter phase (Figure 3b). Referencing the observations to a synthetic/isolation-filter cross-correlation in this fashion allows us to account for interference from unmodeled wave groups and minimizes bias associated with windowing and filtering. We also calculate the sensitivity kernel associated with each phase delay (Figure 3c). These kernels are specific to each observation, and account for interference from unmodeled phases. Such interference can be considerable in data considered here, where the *S* body waves arrive very close in time to the surface wave, and the kernels can differ substantially from standard fundamental-mode surface-wave kernels [*Gaherty et al.*, 1996]. We applied this analysis to all Love and Rayleigh waves with acceptable signal-to-noise ratio. Each observation provides sensitivity to path-average crustal and mantle structure. In general, the five highest frequencies are dominated by structure of the lithosphere, while the 15 mHz band provides sensitivity in the underlying asthenosphere, down to approximately 200 km depth (Figure 3c).

[9] The observations are corrected for a source static derived from the mean observed *P* wave residual estimated for each event, grouped by region and their mean path age, and directly inverted for regional models of upper-mantle shear velocity, as presented in section 3. *P* waves are not

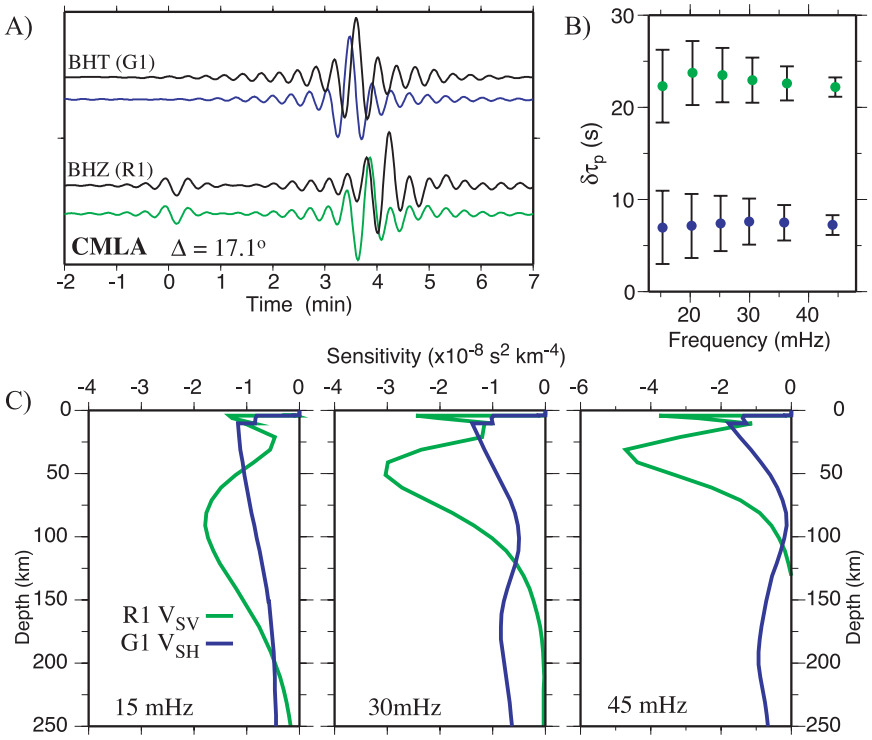

Figure 3. Example of GSDF traveltime analysis. (a) Observed (black) and synthetic (colored) seismograms for a typical source-receiver pair, in this case an MAR event recorded at 17° epicentral distance on station CMLA. Top traces are tangential component waveforms, with Love wave arriving at 3–4 min. Bottom traces are vertical component, dominated by the Rayleigh-wave arrival. Timescale is relative to the predicted *P* wave arrival time. Broadband *P* wave is clearly visible and provides source static for this event. (b) Frequency-dependent phase delays (traveltime residuals) for these two waveforms, measured by cross-correlation between the observed and synthetic waveforms. Blue circles depict frequency-dependent traveltimes of the Love wave, while green circles show phase delays for the Rayleigh wave. (c) Partial-derivative (sensitivity) kernels for both Love and Rayleigh phase delays from Figure 3b in three frequency bands. At 15 mHz the phase delays are sensitive to average velocity structure in the upper 150–200 km, while at higher frequency the sensitivity is concentrated at shallower depths.

clearly visible for some of the events, and no static is applied in those cases. The estimated errors in CMT centroid locations and centroid time are quite small, generally less than ~10 km and 1 s for these events. This error would map into errors in mean shear velocity of <2%, smaller than the differences interpreted here. Most of the models are derived from at least five sources, and it is possible that the traveltime variations due to source errors will average out. Furthermore, the fact that the residuals show predictable age dependence suggests that they are not dominated by source terms.

[10] Figure 4 presents these observations, grouped by region, observation type (Love or Rayleigh), and age. Three important features are discernable in these data. First, it is clear that within each region, the observations show a systematic age dependence: the observations sampling young seafloor exhibit demonstrably larger slownesses than observations sampling older seafloor in the same region. Second, regional variations clearly exist: in particular, the observations at Ascension Island (Figure 4c) are faster (smaller slowness) than those at the Azores (Figure 4b) and along the Kolbeinsey (Figure 4a). Finally, in all cases, Love waves (open symbols) are faster than Rayleigh waves (closed symbols) along the same paths, particularly at intermediate and higher frequency. This is the so-called Love-Rayleigh discrepancy, and it is indicative of upper-mantle anisotropy due to the quasi-horizontal alignment of olivine fabric due to seafloor spreading [*Nicolas and Christensen*, 1987; *Nishimura and Forsyth*, 1988]. The sense of the LR discrepancy (Love faster than Rayleigh) is typical for oceanic regions [e.g., *Nishimura and Forsyth*, 1988; *Gaherty*

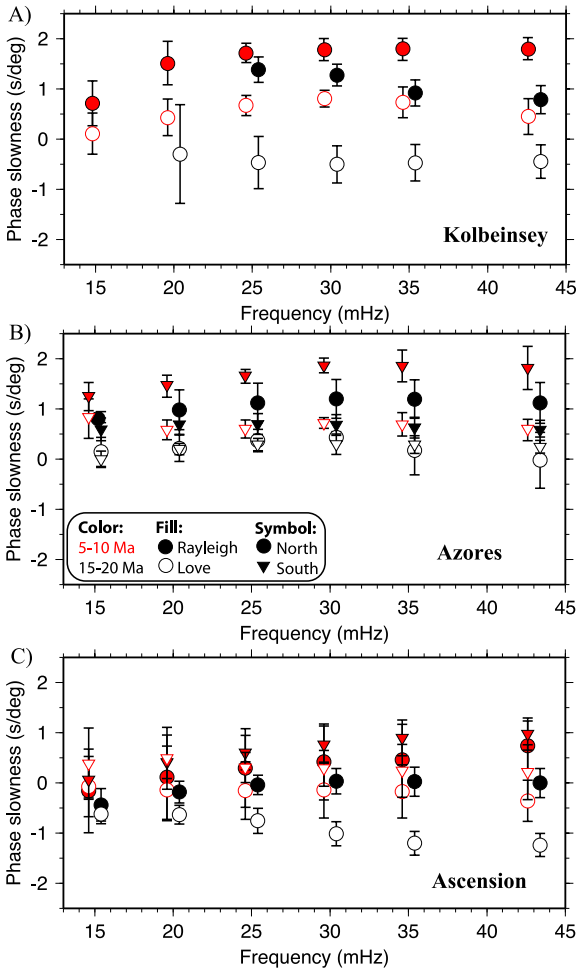

Figure 4. Frequency-dependent phase slowness (phase delays normalized by epicentral distance) relative to an isotropic starting model, corrected for event-specific source statics determined from the average *P* wave residuals. (a) Slowness residuals for Kolbeinsey observations. (b) Slowness residuals for Azores observations. (c) Slowness residuals for Ascension observations. In each panel, individual points represent the mean slowness as a function of frequency, for a given age (red, 0–5 Ma; black, 15–20 Ma), for a given wave type (solid symbols, Rayleigh; open symbols, Love), for a given subregion (circles, paths north of the station(s); triangles, paths south of the station(s)). In all panels the younger (older) observations have been shifted to a slightly lower (higher) frequency to reduce visual overlap. It is clear that (1) Ascension region is characterized by higher velocities relative to the other regions; (2) slownesses along younger paths are always greater than those along older paths in the same region; and (3) Love waves are always faster than Rayleigh waves in the same region.

et al., 1996; *Lévêque et al.*, 1998], but it is the opposite of that observed along the Reykjanes [*Gaherty*, 2001; *Delorey et al.*, 2007]. This suggests that the anomalous, vertically oriented fabric inferred for the Reykjanes is either not present or much less pervasive along the hot spot–influenced ridge segments being analyzed here.

3. Inverse Models of Upper Mantle Shear Velocity

[11] The surface-wave phase delays in each region and age group were inverted for one-dimensional, path-average models of radial anisotropy using a linearized least squares procedure [*Gaherty et al.*, 1996, 1999]. Radial anisotropy represents the simplest parameterization that can satisfy the Love/Rayleigh discrepancy, which requires that horizontally polarized, horizontally propagating waves travel at a different speed than vertically polarized, horizontally propagating waves [e.g., *Dziewonski and Anderson*, 1981]. The resulting models are transversely isotropic and thus cannot explicitly represent the orientation of azimuthal anisotropy most likely associated with seafloor spreading, but they robustly characterize the depth distribution of the anisotropic structure [*Gaherty et al.*, 1999], and the magnitude of the shear anisotropy provides clues to the orientation of the underlying fabric. Large, positive values of shear anisotropy (>3%) indicate fabric that is quasi-horizontal (i.e., olivine-crystal fast axes predominantly lie in a horizontal plane) and oriented oblique to the propagation path [*Nishimura and Forsyth*, 1988; *Gaherty et al.*, 1999]. Small values of shear anisotropy can result from fabric that lacks a strong preferred orientation, as well as fabric that is oriented in the propagation direction. Large negative values of anisotropy suggest predominantly vertical fabric [*Gaherty*, 2001]. To facilitate comparison between structures of different ages and from different regions, we varied only those parameters to which the data were most sensitive, v_{SV} and v_{SH}; inversion tests indicated that compressional-velocity variations were not resolvable.

[12] The models consisted of seven layers between the base of the crust and 250-km depth, with linear changes in velocity within each layer and continuity required across layer boundaries. Crustal thickness along each source-receiver path was fixed at the value specified in Crust2.0 [*Laske et al.*, 2001]. The models are independent of each other, but the use of identical model parameterizations and sim-

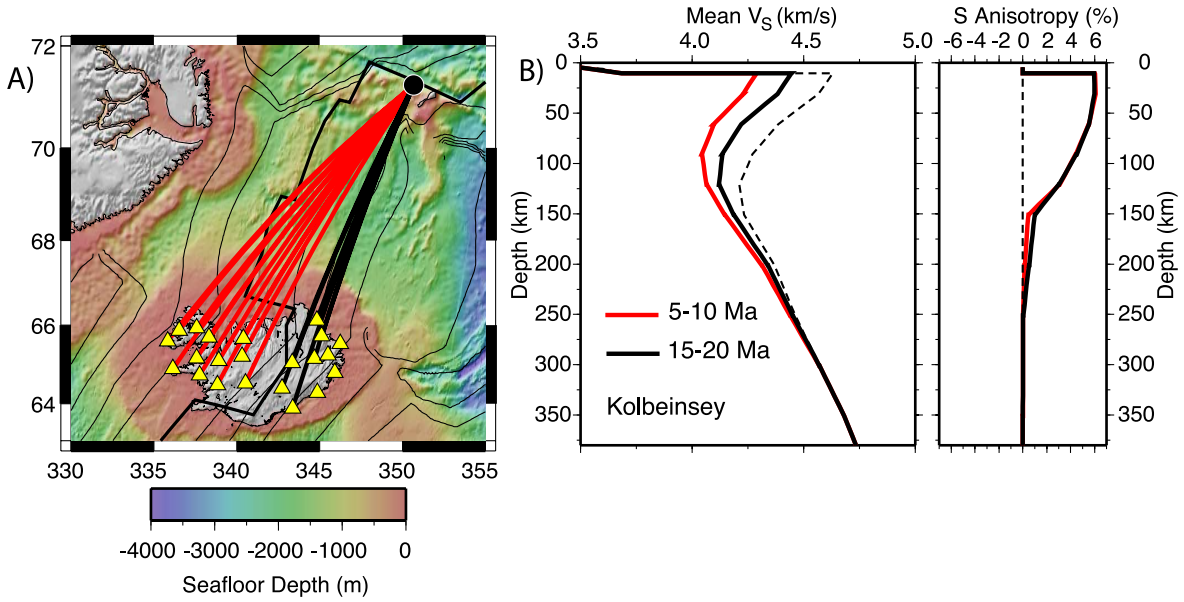

Figure 5. (a) Map of the Kolbeinsey region, showing sources (black circle), receivers (yellow triangles), and raypaths grouped by mean age (red, 5–10 Ma; black, 15–20 Ma). Map provides seafloor bathymetry, using the same scale as in Figure 1. Seafloor age is contoured at 10 Ma intervals. Thick black line shows the plate boundary. (b) (left) Shear velocity and (right) shear anisotropy models derived from the data shown in Figure 5a. Red represents the 5–10 Ma model, and black displays the 15–20 Ma model. Dashed black line shows the starting model. Mean shear velocity and shear anisotropy are defined as in Figure 2.

ilar smoothing and weighting criteria results in very similar forms for the resulting models and no bias due to the parameterization. The age characterization varies by region; the selected source-receiver paths always have mean ages that fall within the specified window (5–10 Ma or 15–20 Ma), but the minimum and maximum ages sampled along those paths can be substantially outside this range (the values for each region are specified in the following subsections). The variance reduction achieved depends on the character of the data and the associated paths; it is high for relatively homogenous paths at short distance (e.g., north of Ascension), while it is lower for more heterogenous paths that are less well represented by a 1-D model (e.g., south of the Azores). However, in all cases the models are able to fit the average character of the surface wave observations (Figure 4), and because of the limitation of our analysis to short source-receiver paths, the spatial resolution of our 1-D models is as good or better than regional tomographic models. Estimated errors in mean shear velocities depend on data quantity and quality, including the robustness of the source statics. A nominal value based on the formal inversion statistics and forward-modeling tests is ±0.03 km/s at depths <75 km, and ±0.04 km/s at depths of 75–150 km, sufficient to infer both age and regional variations within the lithosphere and, to a lesser extent, the underlying low-velocity zone. Radial shear anisotropy is nearly independent of source statics, and is resolved to within better than ±1% over the same depth interval. In general, the precise depth of the velocity minimum within the LVZ, and the velocities below this depth, are not well resolved due to the limited sensitivity depth in these short-arc surface waves (Figure 3).

3.1. Kolbeinsey Ridge

[13] We constructed shear-velocity models of upper-mantle structure in two lithospheric age intervals (5–10 Ma, and 15–20 Ma) using HOTSPOT recordings from a single event from near Jan Mayan (Figure 5). The source-receiver geometry is very effective in isolating age-dependent lithospheric structure, albeit at short epicentral distances (6–8°). As a result, the observations at the southern stations have substantial portions of their propagation paths within Iceland. We reduce the impact of this sampling by preferentially weighting the observations from the northernmost stations. The 5–10 Ma model is based on 130 delay-time observations from 12 stations, with actual mean path

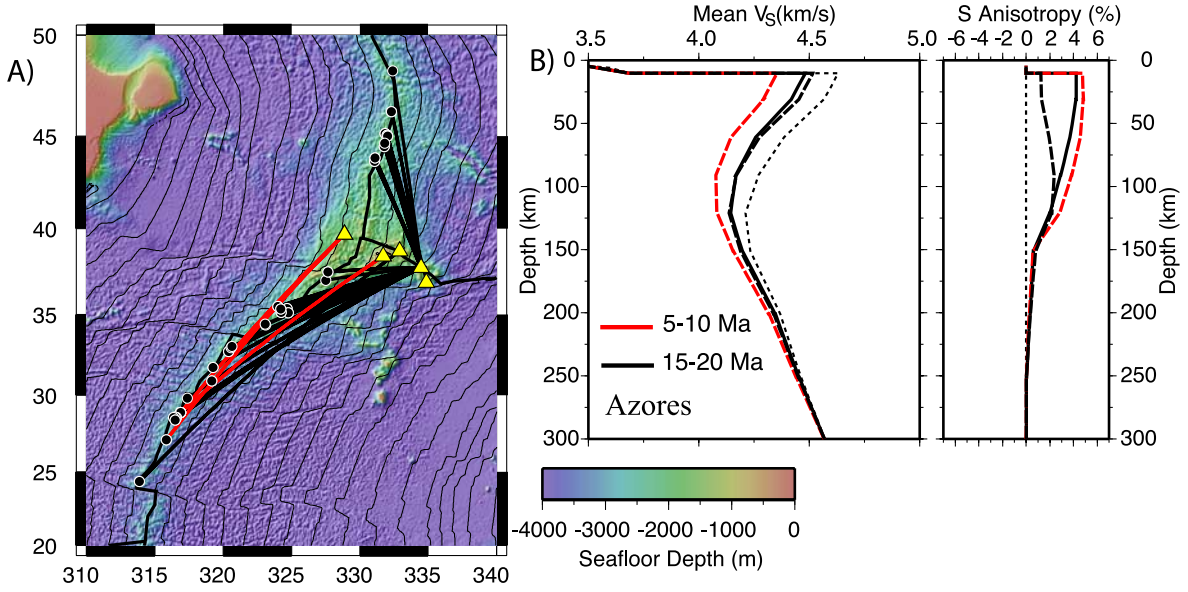

Figure 6. (a) Map of the Azores region, showing sources (black circle), receivers (yellow triangles), and raypaths grouped by mean age (red, 5–10 Ma; black, 15–20 Ma). Map provides seafloor bathymetry, using the same scale as in Figure 1. Seafloor age is contoured at 10 Ma intervals. Thick black line shows the plate boundary. (b) (left) Shear velocity and (right) shear anisotropy models derived from the data shown in Figure 6a. Red represents the 5–10 Ma model, and black displays the 15–20 Ma model. Dashed lines represent models for south of Azores, while solid lines represent north Azores models. Thin dotted black line shows the starting model. Mean shear velocity and shear anisotropy are defined as in Figure 2.

ages ranging from 5–9 Ma and minimum and maximum ages sampled along these paths of 0 and 18 Ma, respectively. The 15–20 Ma model is derived from 54 observations from 6 stations, with mean path ages spanning 16–20 Ma, and minimum and maximum age sampling of 5 and 31 Ma.

[14] We were able to estimate an average *P* wave source static using observations from several stations, and Figure 5 presents the models resulting from inversion of the data using this static. The age dependence is clear, and each model is faster than the Reykjanes model from the comparable age interval. The shear anisotropy is relatively strong in both models (~5%) and positive above ~150 km depth, which is very different than the Reykjanes models.

[15] In these models, we opted not to utilize two additional Jan Mayan events recorded by HOTSPOT. These events provided energetic Rayleigh-wave observations, but Love waves from these events had very poor signal-to-noise levels. We could have used the Rayleigh wave observations from these events, but we chose not to for two reasons. First, because the observations are accompanied by an additional (relatively unknown) source static, inversion tests indicated that the additional observations did not improve our ability to resolve differences as a function of age. Second, the anisotropy estimates are derived from the difference between models of v_{SH} and v_{SV}. Since v_{SH} is constrained entirely by Love waves, and v_{SV} is constrained primarily by Rayleigh waves, a large mismatch between the Love and Rayleigh data sets could lead to substantial bias in the anisotropy estimates. The downside of this decision is that the models (Figure 5) are dependent on a single source, so that uncertainties in mean v_s are slightly larger than the nominal values (~±0.05 km/s). We do note that the Rayleigh wave delays measured for all three events were broadly consistent, suggesting that the event parameters of the chosen event were not anomalous.

3.2. Azores Region

[16] Using observations recorded at permanent station CMLA, combined with temporary stations COV2, PSJO, PSCM, and PSMA of the MIDSEA experiment, we derived models for structure both north and south of the Azores (Figure 6). CMLA, PSCM, and PSMA sit off-axis to the east of the MAR, nearly astride the Eurasia-Africa plate boundary on seafloor with approximate age of 20–50 Ma. They are useful for deriving models

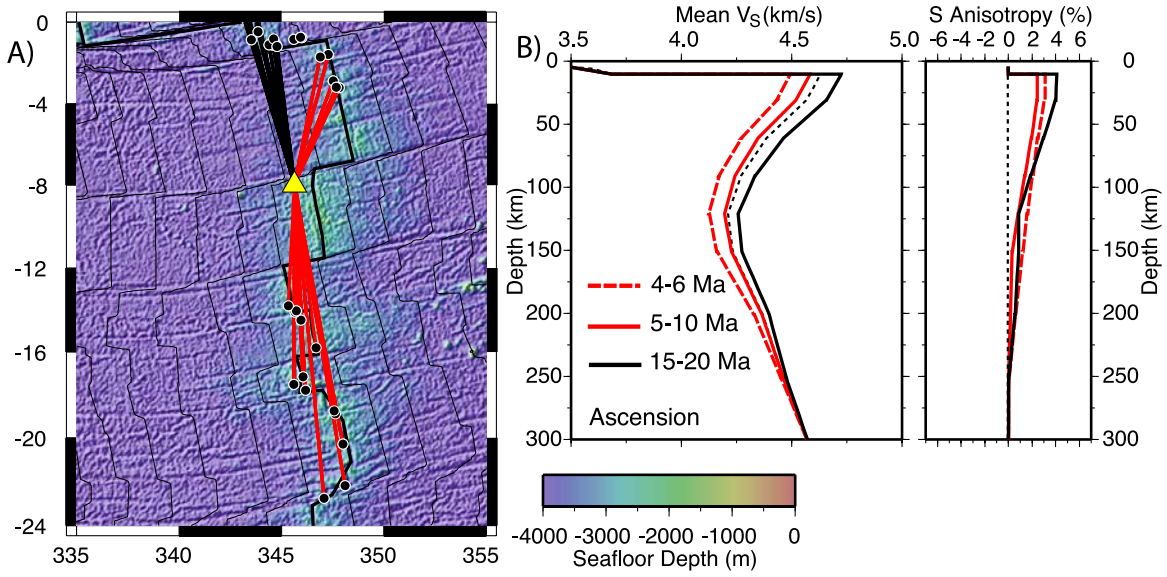

Figure 7. (a) Map of the Ascension region, showing sources (black circle), receivers (yellow triangles), and raypaths grouped by mean age (red, 5–10 Ma (north) and 4–6 Ma (south); black, 15–20 Ma). Map provides seafloor bathymetry, using the same scale as in Figure 1. Seafloor age is contoured at 10 Ma intervals. Thick black line shows the plate boundary. (b) (left) Shear velocity and (right) shear anisotropy models derived from the data shown in Figure 7a. Solid red and solid black lines represent north Ascension 5–10 Ma and 15–20 Ma models, respectively. Dashed red lines represent south Ascension 4–6 Ma model. Thin dotted black line shows the starting model. Mean shear velocity and shear anisotropy are defined as in Figure 2.

with average age in the 15–20 Ma interval using several MAR events both north and south of the hot spot. PSJO and COV2 are both located closer to the ridge axis, and during the MIDSEA deployment they recorded two MAR events from the south that provide high S/N Rayleigh and Love waves along paths with mean age between 5–10 Ma. North of the Azores, the 15–20 Ma model was derived from 102 measurements from 10 events, with mean path ages ranging from 16–21 Ma and minimum and maximum ages sampled along these paths of 0 and 48 Ma, respectively. South of the Azores, the 5–10 Ma model was constrained by 36 observations from two events, with mean path ages of 6–9 Ma and minimum/maximum sampled ages of 0/18 Ma. The 15–20 Ma model was produced from 195 observations from 19 events, with mean path ages of 15–20 Ma and minimum and maximum ages sampled along these paths of 0 and 42 Ma, respectively.

[17] The age dependence is clear in the models from the south of the Azores, with the 15–20 Ma model being approximately 4% faster than the 5–10 Ma model. On the basis of the 15–20 Ma models, there is no resolvable difference in the mean shear velocity north and south of the hot spot. Overall, the velocities are higher than the Reykjanes models of the same lithospheric age. There are discernable variations in radial shear anisotropy within the region, with the anisotropy at 15–20 Ma south of the Azores being substantially smaller (~2–3%) than the other two models (~5%). This discrepancy can be seen directly in the delay times (Figure 4), and the difference between the two 15–20 Ma models (north and south of the Azores) appears to be particularly robust, as the models are derived from comparable number of observations. The difference in anisotropy between the two south Azores models is less well quantified. While the magnitude of the anisotropy in the 5–10 Ma model is consistent with the substantial Love-Rayleigh discrepancy observed in the delay times, it is derived from only four source-receiver paths, less than one-quarter of that used for the 15–20 Ma model.

3.3. Ascension Region

[18] Using observations recorded at GSN station ASCN, we derived models for structure both north and south of the Ascension Island hot spot (Figure 7). ASCN sits off-axis just west of the MAR and just south of the Ascension fracture zone.

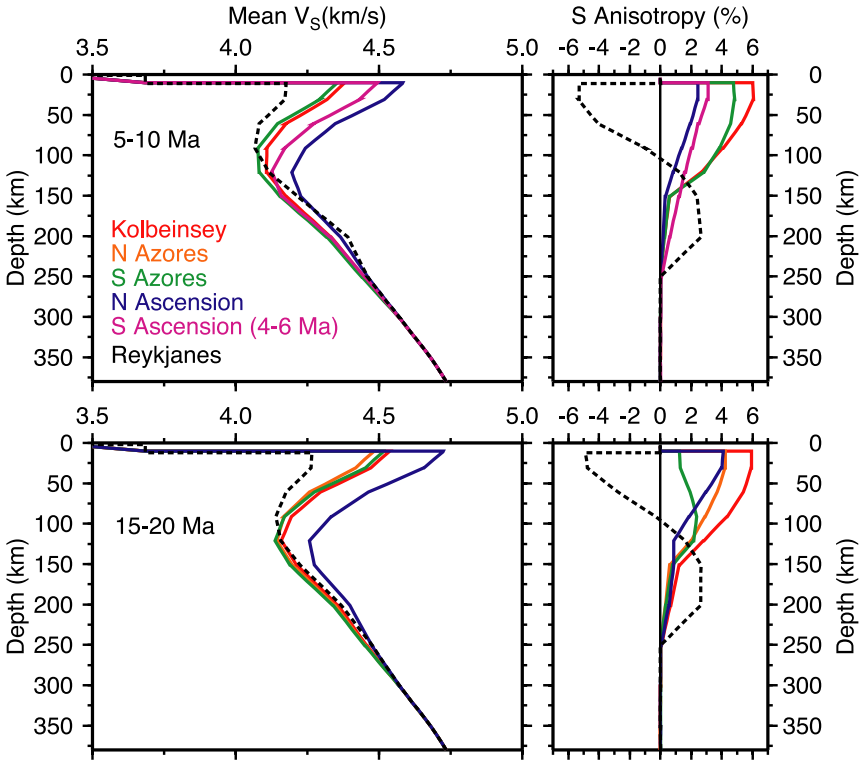

Figure 8. Mean shear velocity and shear anisotropy (as defined as in Figure 2) for all regions, grouped by mean age. Colored traces show Kolbeinsey, Azores, and Ascension models presented in Figures 5–7; black dashed line displays Reykjanes models of *Gaherty* [2001] in comparable age intervals. Top panels show models for 5–10 Ma (S. Ascension model is for 4–6 Ma); bottom panels show models for 15–20 Ma.

Beneath and directly south of the station, seafloor age is approximately 7 Ma, while directly north of the station (and the fracture zone) the crustal age is approximately 18 Ma (Figure 7). South of ASCN, 13 MAR events provided 138 surface-wave delay times with path-average ages in the narrow range of 4–6 Ma (minimum and maximum ages sampled are 0 and 16 Ma). North of ASCN, six MAR events produced 60 observations in the 5–10 Ma interval; path-average ages range from 6 to 10 Ma, with minimum/maximum sampled ages of 0/17 Ma. Eight events provided 90 observations in the 15–20 Ma age range, with average path ages spanning 15–17 Ma, and minimum and maximum sampled ages of 0 and 26 Ma, respectively.

[19] The average shear velocity models are faster than the models at comparable age from other regions. The age dependence is clear in the models from the north of Ascension, with the 15–20 Ma model being approximately 3% faster than the 5–10 Ma model. The structure south of ASCN is not sampled in a comparable age interval, so variations in structure between the southern and northern paths cannot be assessed. The 4–6 Ma model for the southern paths is 2% slower than the northern 5–10 Ma model, consistent with lithospheric cooling. This difference may reflect other structural differences as well. The radial shear anisotropy varies slightly within the region, with smaller values (2–3%) observed at the younger ages relative to that observed at 15–20 Ma (~4%). In all age intervals, the anisotropy below approximately 50-km depth appears to be somewhat weaker than that found in the other regions.

4. Temperature and Compositional Variations Along the MAR

[20] The shear velocity models display significant regional variations in both mean v_S and radial anisotropy (Figure 8). This structural heterogeneity is also seen in upper-mantle tomography models from the region [e.g., *Silveira and Stutzmann*, 2002; *Pilidou et al.*, 2004], and it is likely due in part to variations in mantle temperature. Globally, along-axis temperature variations of up to 150°K are suggested by compositional trends of MOR basalts [*Klein and Langmuir*, 1987], while in the

Atlantic, variations in seismic traveltimes suggest temperature variations of order 100°K averaged over the upper 300 km of the mantle [*Sheehan and Solomon*, 1991]. Detailed tomographic studies of Iceland indicate localized temperature perturbations of order 200°K [e.g., *Allen et al.*, 2002; *Li and Detrick*, 2006] and a seismic study of the asthenosphere underlying the Reykjanes ridge [*Delorey et al.*, 2007] reveals temperature perturbations of 50–75°. In accord with the latter results, crustal-thickness variations [*White*, 1997] and numerical models of hot spot–ridge interaction [*Ito*, 2001] suggest that high-temperature plume anomalies of order 50–100°K can persist hundreds of kilometers down the Reykjanes ridge.

[21] Direct inference of temperature variations from seismic data is often difficult in ridge and hot spot environments, however, due to the competing effects of melt and temperature [e.g., *Hammond and Humphreys*, 2000; *Dunn and Forsyth*, 2003; *Li and Detrick*, 2006]. Our models provide an alternative means to quantify thermal variations along the ridge axis, specifically by evaluating the age-dependent velocity structure in the oceanic lithosphere. Oceanic lithosphere is particularly useful because it is free of melt, and its age-dependent thermal structure can be predicted using well-calibrate thermal models [e.g., *Parsons and Sclater*, 1977; *Stein and Stein*, 1992; *Carlson and Johnson*, 1994]. In the following subsections, we explore several likely explanations for the shear-velocity variation observed in Figure 8.

4.1. Half-Space Cooling With Regional Variations in Mantle Temperature

[22] We first consider simple half-space cooling of oceanic lithosphere, with regional velocity variations driven by fluxuations in mantle (potential) temperature. Within the individual Atlantic regions, the increase in mean v_S as a function of lithosphere age is qualitatively consistent with the notion of plate- or half-space cooling of oceanic plates. However, as shown in Figure 8, there is also a strong regional variation of models with similar average age. Ascension models are systematically faster than the other regions above ~100 km depth in both age intervals. The Kolbeinsey and both regions north and south of Azores have mantle velocities that are indistinguishable within error; and the Reykjanes models are systematically slow above ~100 km depth compared to the other regions. In all cases, the regional variations are clear through the lithosphere, which should have a thickness of order 30–60 km, defined either thermally (e.g., the 650°C isotherm of *Anderson* [1989]) or compositionally [*Hirth and Kohlstedt*, 1996], across these age intervals. The variations persist into the underlying asthenosphere.

[23] If we assume that the lithospheric velocities are controlled by half-space or plate cooling, then the regional velocity variations shown in Figure 8 may result from potential temperature fluctuations beneath the ridge axis and the adjacent lithosphere. Figure 9 displays a test of this hypothesis. For each model, we calculate the mean mantle v_S between the Moho and 40-km depth (dubbed V_S^{40}). Likewise, we calculate the mean temperature T^{40} over the same depth range, assuming a half-space cooling model [*Turcotte and Schubert*, 2002] with potential temperature of 1350°C and seafloor age determined by the mean of the propagation-path ages. These values provide empirical measures of velocity versus temperature for several ages in each of the five regions along the MAR, plus the Reykjanes region using the models of *Gaherty* [2001] (Figure 9a). These observations can be compared to similar observations calculated from age-dependent upper-mantle shear-velocity models from fast spreading Pacific lithosphere [*Nishimura and Forsyth*, 1988; *Gu et al.*, 2005], as well as theoretical calculations of shear-velocity versus temperature, $V_S(T)$, that are based on laboratory estimates of shear attenuation [*Jackson et al.*, 2002] combined with an analytical model of anelastic dispersion that specifies $\delta V_S/\delta T$ due to shear attenuation [*Karato*, 1993]. These calculated $V_S(T)$ curves assume values for several physical constants that are specified by *Karato* [1993] and *Jackson et al.* [2002], and they are based on the assumption that velocity variations are driven entirely by temperature variations in a solid-state peridotite mantle; the effects of water and/or melt are excluded. Two critical free parameters in this calculation are the grain size of mantle rock (which controls the rate of roll-off of the velocity curve at high T), and a reference value v_S at a reference temperature T_0, to which the $\delta V_S/\delta T$ perturbations are applied. The gray band in Figure 9a represents a reasonable range of grain size (~1–10 mm) and a range of reference velocities chosen to roughly fit the velocities for the Pacific models at low temperatures ($V_S \sim 4.4$ km/s at $T_0 \sim 800$°C). *Gu et al.* [2005] used a similar formulation to quantitatively test for the impact of melt on near-axis velocities in the Pacific. In our case, it is likely that melt is not a critical issue at these ages and depth ranges, and the theoretical velocity-temperature relationship

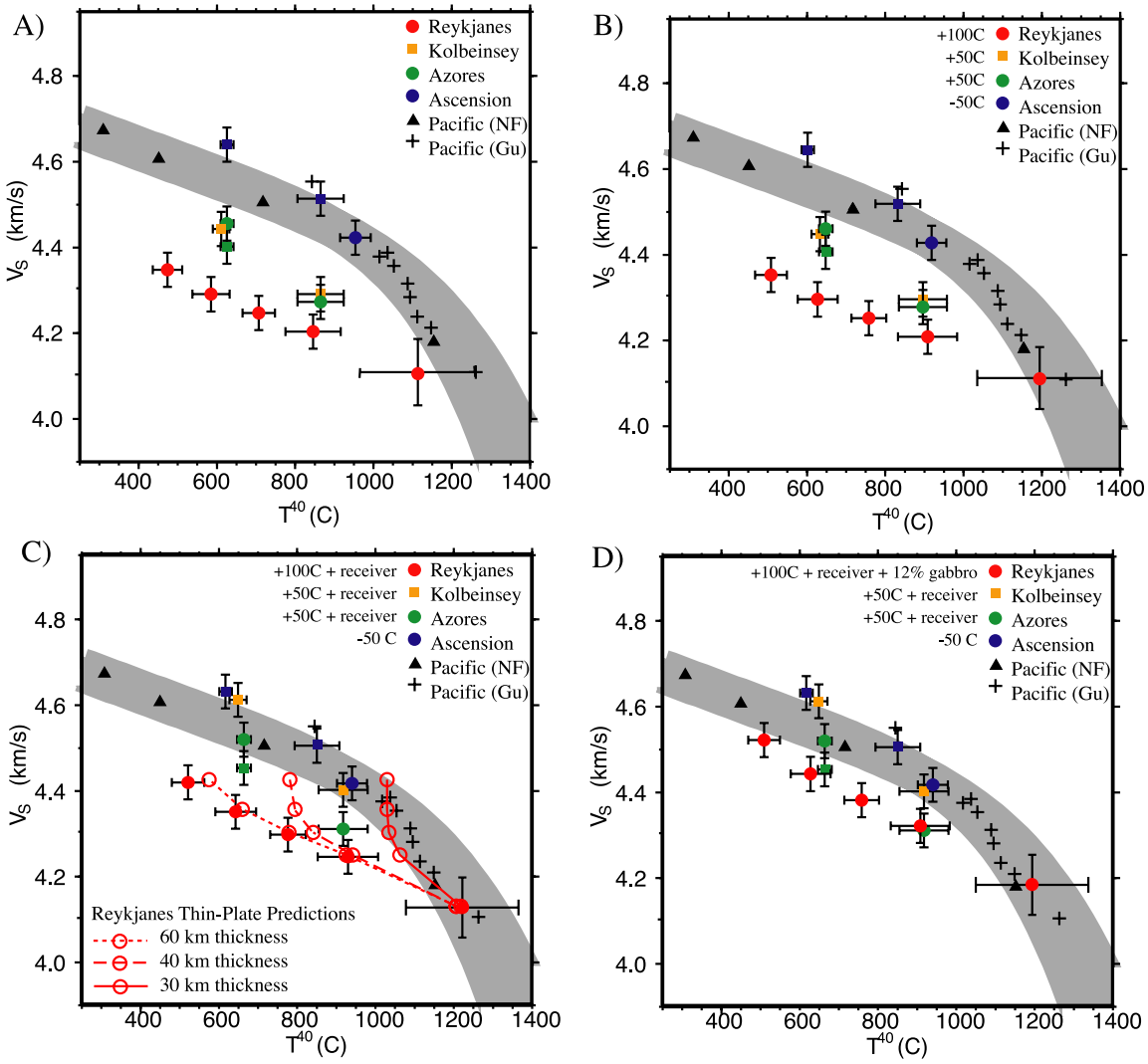

Figure 9. Mean mantle shear velocity (V_S^{40}) versus mean temperature (T^{40}) in the upper 40 km derived from the MAR models in Figure 8 (colored symbols). Circles represent "south" models, while squares represent "north" models. The MAR estimates are compared to similar estimates calculated from shear-velocity models of Pacific lithosphere (black symbols) (NF, *Nishimura and Forsyth* [1988]; Gu, *Gu et al.* [2005]), and to theoretical calculations of $V_S(T)$ for solid-state peridotite (gray band), as described in the text. For all calculations, temperature as a function of depth and seafloor age is determined using a half-space cooling model with a half-space temperature of 1350°C. Half-space cooling estimates of T^{40} are indistinguishable from a plate model [e.g., *Stein and Stein*, 1992] for plate thicknesses of 80 km and greater. Models of shear velocity and temperature are averaged between the base of the Moho and 40 km depth beneath the solid surface. Error bars on V_S^{40} are approximate; error bars in T^{40} represent one standard deviation in the temperature range spanned by the age range. (a) Raw estimates of V_S^{40} and T^{40}. (b) Raw estimates of V_S^{40}, plotted against T^{40} estimates where the MAR models have regionally variable half-space (mantle) temperatures that range from −50 C to +100 C relative to the Pacific models. (c) Estimates of V_S^{40} for the northern MAR corrected for a low-velocity region beneath Iceland and the Azores. Corrected velocity is calculated by assuming a 200-km radius region of 4.0 km/s centered beneath the stations, and Voight averaging of the velocities along the mean path length for each region. T^{40} estimates are the same as in Figure 9b. Also shown in red circles and lines are T^{40} estimates for the Reykjanes models, assuming several thin-plate models, as described in the text. Plate-model temperatures are calculated using the formulation of *Stein and Stein* [1992] and assume an asthenosphere temperature of 1450°C. (d) Same as Figure 9c, but with V_S^{40} for the Reykjanes models further "corrected" for the effects of 12% gabbro. Velocity of gabbroic component is taken to be 3.75 km/s [*Mooney et al.*, 1998].

simply provides a baseline to facilitate the comparison of our regional models.

[24] A number of inferences can be drawn from Figure 9a. First, within each region, the increase in velocity with increasing age (decreasing T^{40}) roughly follows the slope predicted for solid-state temperature dependence of velocity away from the high-T (near solidus) roll-off. Thus it is reasonable to interpret the velocity-age relationship within each sub-region in terms of lithospheric cooling, in the absence of melt. If we assume that the theoretical velocity-temperature curve represents "typical" oceanic lithosphere [see also *Faul and Jackson*, 2005; *Priestley and McKenzie*, 2006], then the Ascension models are slightly faster than or indistinguishable from average, the Kolbeinsey and Azores region are slower than average, and the Reykjanes lithosphere is extremely slow. This inverse correlation between apparent hot spot flux and mantle velocity suggests that hot spot volcanism is fundamentally related to upper-mantle source variations over length scales that are a substantial fraction of the seismic path lengths, certainly several hundred kilometers. It is almost certainly driven in part by temperature variations in the mantle source, and Figure 9b explores the degree to which a plausible range in mantle potential (half-space) temperature can explain the observations. In Figure 9b, the T^{40} estimates for each model have been calculated using a regional perturbation to the ridge potential temperature: $\Delta T = -50$ K for the Ascension models, $\Delta T = +50$ K for Azores and Kolbeinsey, and $\Delta T = +100$ K for Reykjanes. The half-space cooling assumption implies that these temperature perturbations are steady state between 5–20 Ma, and span a region from the ridge to 20 Ma seafloor, i.e., they represent the temperature of the ridge and the underlying asthenosphere throughout the cooling history of the lithosphere. These values span much of the temperature range inferred for the global ridge system from geochemistry [*Klein and Langmuir*, 1987], and thus are probably larger that would be expected for the MAR, especially given that the models represent average velocity (and thus temperature) over 600–2000 km of ridge length. Nevertheless, these regional perturbations provide a quantitative test of mantle temperature as the mechanism for the observed velocity variation.

[25] Figure 9b suggests that the full range in observed velocities is too large to be explained solely by temperature in this half-space-cooling scenario. A low-temperature mantle source ($\Delta T \sim -50$ K) can explain the relatively high velocities observed near Ascension Island (although the agreement with the theoretical range is only slightly improved over the case of no temperature perturbation), but the velocities near the north Atlantic hot spots remain ~0.05–0.15 km/s lower than predicted even for a moderately high-temperature ridge source ($\Delta T \sim +50$–100 K). Furthermore, it is clear that a simple adjustment to half-space temperature (no matter how large) cannot shift these models into agreement with the theoretical curve or the Pacific models. Regional variations in mantle potential temperature move the points in Figure 9 along the horizontal axis, and because of the nonlinearity of the temperature-age relationship, the largest horizontal shifts occur for the youngest-age models (the highest-temperature points in Figure 9). The Reykjanes, Kolbeinsey, and Azores models retain anomalously slow velocities out to the oldest age, making it impossible for this model to explain them.

4.2. Contribution of Three-Dimensional Thermal Processes

[26] This calculation may underestimate the thermal impact of the hot spot sources on the lithosphere velocity estimates due to three-dimensional effects. The path-average shear velocities may be biased low due to strong 3-D heterogeneity, possibly associated with partial melt, beneath the hot spot stations. Regional tomography indicates velocities as low as ~4.0 km/s in the upper 150-km of the mantle, extending up to 200-km radius from the center of both Iceland and the Azores [*Allen et al.*, 2002; *Pilidou et al.*, 2004; *Li and Detrick*, 2006]. Figure 9c explores the degree to which such structure can explain the slow velocities. Assuming that our path-average models integrate such heterogeneity into the structure, we correct the V_S^{40} estimates by removing the contribution of a 200-km radius low-velocity (4.0 km/s) column to the path-average velocities (Figure 9c). These receiver-corrected terms, combined with +50 K mantle temperature perturbation, are sufficient to bring the average lithospheric velocities observed along the Kolbeinsey and near-Azores ridges into agreement with the Pacific and theoretical estimates.

[27] Even with these corrections, the Reykjanes observations remain outliers at all but the youngest age (Figure 9c). This may be because the T^{40} estimates (based on half-space cooling) are too low, rather than the velocities being anomalously slow. A plausible scenario is that the episodic

flushing of the sublithospheric mantle with hot plume material from Iceland [e.g., *Vogt*, 1971; *Ito*, 2001] convectively reheats the cooling lithosphere. The v-shaped ridges along the RR suggest that plume material may propagate down the ridge at ~10 times the half-spreading rate [*White et al.*, 1995], and if such flow occurs in the sublithospheric mantle, it may be quite effective in thermally eroding or otherwise destabilizing the base of the lithosphere. We can approximate this process by characterizing the lithospheric cooling using a "plate" model [e.g., *Parsons and Sclater*, 1977; *Stein and Stein*, 1992], which imposes a maximum depth of the base of the conductive lithosphere and thus effectively presumes advective heat transport below this depth. Figure 9c shows three scenarios where T^{40} for the Reykjanes models is calculated via a plate model [*Stein and Stein*, 1992] with sublithospheric temperature of 1450°C and plate thicknesses of 60 km, 40 km, and 30 km. A very thin plate only 30-km thick brings the RR observations into accord with the theoretical predictions and other regions. While this model is plausible, we do not feel that it is likely for two reasons. First, there is little evidence for such a thin plate east of the Reykjanes on the Eurasian plate, which these models represent. *Delorey et al.* [2007] find that the Eurasian-plate lithosphere thickens progressively to ~60 km depth at an age of ~30 Ma, and *Heller and Marquart* [2002] find that the admittance along profiles east of the RR can be well-modeled using a half-space cooling approximation. (In both cases, the lithospheric structure west of the ridge is found to be anomalous, but that region is not represented by the models presented here.) Second, while this thin-plate model can explain the overall slow velocities, it cannot explain the monotonic increase in V_S^{40} for models with ages >15 Ma. T^{40} reaches a minimum asymptote at ~1100 C at this age, and does not decrease further with age (Figure 9c). If temperature were the sole control on velocity, then one would expect the velocity structure to reach a similar asymptote.

4.3. Evidence for Hot Spot–Induced Compositional Heterogeneity

[28] We consider the possibility that that the anomalously slow velocities in the north Atlantic reflect compositional heterogeneity emplaced in the lithosphere at the hot spot–affected ridges. Compared to normal MOR lithosphere, the mantle lithosphere near Iceland and the Azores is likely to be more depleted of basaltic components due to larger extents of melting [e.g., *Langmuir et al.*, 1993]. The resulting impact on seismic velocities is probably minimal [*Schutt and Lesher*, 2006], and it is opposite in sign to that needed to explain our observations (greater depletion increases velocities). However, it is commonly observed that peridotites from slow spreading lithosphere contain substantial quantities of embedded gabbro [e.g., *Cannat et al.*, 1992; *Kelemen et al.*, 2004]. These gabbroic inclusions in oceanic mantle lithosphere suggest that the melt extraction process at mid-ocean ridges is not necessarily 100% efficient; conditions may exist in which the rate of melt production exceeds the accompanying rate of melt extraction [*Cannat*, 1996]. This may be particularly true at slow seafloor-spreading rates, where conductive cooling near the ridge crest might significantly reduce the rate of extraction [*Lizarralde et al.*, 2004].

[29] In our case, we envision that the enhanced melt productivity associated with the high-temperature hot spot source at Iceland cannot be accommodated by normal extraction processes along the slow-spreading segments of the MAR. The retained melt crystallizes as gabbro in the sub-Moho upper mantle. This process may be quasi-steady state, occurring persistently over the ~40 Ma history of hot spot influence on the RR. Alternatively, it may be triggered periodically by pulses of enhanced plume flux moving down the ridge, as proposed by *Ito* [2001] to explain the v-shaped ridges observed in seafloor bathymetry and gravity [e.g., *Vogt*, 1971; *Jones et al.*, 2002]. The enhanced melting may produce not only thickened crust beneath the v-shaped ridges [*Jones et al.*, 2002], but increased gabbro content in the underlying mantle. This latter scenario is particularly attractive if one assumes that, averaged over a timescale appropriate for mean oceanic crust production (several Ma), the melt production and melt extraction associated with normal seafloor spreading are balanced in a quasi-steady state equilibrium. The introduction of a high-temperature plume pulse such as that modeled by *Ito* [2001] (~8 Ma periodicity) could upset this balance, producing an increase in melt production that cannot be fully accommodated by the melt-extraction system over this timescale. This notion is conceptually similar to that suggested by *Lizarralde et al.* [2004], in that the anomalous retention of gabbro is spurred by an abrupt perturbation to the melt production and extraction system.

[30] Figure 9d presents a test of the retained-gabbro hypothesis. Even after other corrections, the Reykjanes velocities are low by of order 0.1 km/s.

Assuming typical velocities for gabbro, this velocity anomaly suggests approximately 12% (by volume) gabbro in the Reykjanes lithosphere, distributed throughout the upper 40 km. "Correcting" for this structure brings the Reykjanes velocities into the range with the other regions and the thermal predictions, albeit at the lower edge of this range (Figure 9d). Further increasing either the amount of gabbro, or the thermal anomaly, would push the predictions comfortably into range with the other regions. The compositional heterogeneity may contribute to the shallow bathymetry and negative gravity anomaly throughout the RR region, which are both suggestive of lower-density lithosphere. Thicker crust and/or warmer sublithospheric mantle are generally invoked to explain these signals [e.g., *Heller and Marquart*, 2002; *Delorey et al.*, 2007], but low compositional densities may also contribute.

[31] The presence of upper-mantle gabbro is fully consistent with the notion that hot mantle temperatures should produce excess quantities of basaltic melt [e.g., *McKenzie and Bickle*, 1988; *Kinzler and Grove*, 1993; *Langmuir et al.*, 1993]. On the basis of relative shear velocities across the region, *Delorey et al.* [2007] estimate an asthenospheric temperature anomaly of +50–75 C, consistent with along-axis temperature anomalies of up to +100 C estimated from geochemistry [e.g., *Ito et al.*, 2003]. Using standard mantle melting models [*McKenzie and Bickle*, 1988; *Kinzler and Grove*, 1993], we estimate that temperature anomalies of 50–100 K will produce 4–9 km of "excess" basaltic melt. Approximately 3–4 km of this excess melt appears to make it into the crust; average crustal thickness along the Reykjanes is ~10 km, compared to typical oceanic crust of ~6–7 km [*White*, 1997]. This leaves up to 6 km of excess basalt for distribution elsewhere. Our estimate of 12% retained gabbro over a 40-km depth requires the equivalent of approximately 5 km of crust, in good agreement with the available excess.

[32] The evidence for this compositional anomaly is strongest along the RR. The Kolbeinsey and Azores ridges also are quite slow relative to the Pacific and theoretical predictions. While the more extreme temperature and near-station corrections can potentially explain these signals (Figure 9c), it is possible that retained gabbro may contribute to the slow lithosphere observed in these regions (the south Azores at 5–10 Ma stands out as particularly anomalous). Along Kobleinsey, the influence of the Iceland hot spot on ridge processes is evident in crustal thickness [*Hooft et al.*, 2006] and geochemical [e.g., *Blichert-Toft et al.*, 2005] observations. Likewise, the MAR near the Azores exhibits evidence of hot spot influence, both in basalt chemistry [*Dosso et al.*, 1999] and in the presence of v-shaped ridges south of the archipelago [*Escartin et al.*, 2001]. These observations suggest hot spot–enhanced melting are occurring in these regions, and melt retention may contribute to the slow lithospheric shear velocities.

5. Radial Anisotropy Variations Along the MAR

[33] The radial anisotropy models summarized in Figure 8 also display regional variations that suggest different flow processes beneath the six stretches of the MAR. In general, anisotropic velocities in the oceanic lithosphere are interpreted in terms of lattice-preferred orientation (LPO) of olivine in the mantle, with the olivine ***a*** axes preferentially aligned quasi-horizontally in the seafloor-spreading direction [e.g., *Hess*, 1964; *Nishimura and Forsyth*, 1988; *Gaherty et al.*, 2004]. Sampling of such fabric by surface waves traveling roughly ridge-parallel would produce models of radial shear anisotropy with a large, positive magnitude (>~3%) in the lithosphere. An exception was found along the Reykjanes Ridge, where large negative values of shear anisotropy suggest fabric with a strong near-vertical orientation [*Gaherty*, 2001; *Delorey et al.*, 2007]. The models presented here for other sections of ridge show no sign of this vertical fabric, including along the Iceland-influenced Kolbeinsey ridge (Figure 8). This suggests that, to first order, the anisotropy reflects quasi-horizontal fabric in the oceanic lithosphere produced by corner flow at the ridge. The Reykjanes models were interpreted in the context of hot spot–fueled buoyancy-driven upwelling beneath the ridge axis; if this interpretation is correct, such a process appears to be weak or rare, even on ridge segments where hot spot influence is otherwise apparent.

[34] The observed variations in magnitude imply differences in the near-axis mantle deformation field between the regions. At 5–10 Ma, the shear anisotropy along both Ascension segments is weaker (~3 ± 1%) than that along Kolbeinsey and N. Azores (~5 ± 1%). Given that the mean shear velocities near Ascension are suggestive of "normal", relatively low-temperature ridge conditions (section 4.1), one possibility is that the weak anisotropy is due to inefficient alignment of olivine

fabric in slow spreading systems [*Gaherty et al.*, 2004]. In contrast, the ridge segments that show a stronger hot spot influence in mean v_S also have larger-magnitude anisotropy, suggesting that the hot spots produce relatively strong deformation (and thus fabric) in the near-ridge mantle.

[35] The observations at 15–20 Ma are somewhat supportive of this notion; the N. Ascension model has relatively weak anisotropy, although the difference between N. Ascension and N. Azores is not resolvable. The anisotropy along Kolbeinsey is relatively strong. The shear anisotropy at 15–20 Ma in the S. Azores region is markedly different than the other regions; it is also quite different than the anisotropy observed at younger age in the same region. Specifically, the anisotropy in this model is very weak (~1–2%) above ~75 km depth. It is not easy to explain these differences as being due to variations in mantle dynamics. The hot spot activity that produced the Azores platform occurred between ~5–14 Ma [*Cannat et al.*, 1999; *Escartin et al.*, 2001], and thus the 15–20 Ma models from S. and N. Azores should reflect comparable (normal slow spreading) conditions. The plume influence on the adjacent MAR after 14 Ma was strongest to the south, however [*Cannat et al.*, 1999], and the raypaths used in constructing the 15–20 Ma S. Azores models clearly sample the hot spot–affected region. Thus it is possible that the weakened anisotropy along this path reflects significant reorganization or modification of the uppermost mantle fabric due to hot spot–induced flow, similar to, but much weaker than, the modification suggested for the Reykjanes [*Gaherty*, 2001]. The weak anisotropy may also be result from two geometric biases, however. First, a number of the short-distance paths included in the S. Azores 10–15 Ma models travel nearly parallel to the fossil spreading direction. The small traveltime differences observed along these paths are consistent with an azimuthal anisotropy oriented with fossil spreading [*Maupin*, 1985]. Second, the S. Azores 10–15 Ma models include several longer (15–20°) raypaths that sample seafloor formed well south of the inferred extent of hot spot influence. This segment of normal seafloor may reduce the average magnitude of shear anisotropy within the region.

6. Conclusions

[36] We probe variations in temperature, composition, and mantle fabric in oceanic lithosphere formed along hot spot–influenced sections of the Mid-Atlantic Ridge, using surface waves from nearby ridge earthquakes recorded on island-based broadband seismic stations. Mean shear velocity profiles in the upper 150 km of the mantle correlate with apparent hot spot flux: lithosphere formed near the low-flux Ascension hot spot is characterized by relatively high mantle velocities, while the MAR near the higher-flux Azores hot spot has lower velocities. The impact of the high-flux Iceland hot spot on mantle velocities along the nearby MAR is strongly asymmetric: the lithospheric velocities near the Kolbeinsey ridge are moderately slow (similar to those near the Azores), while velocities near the Reykjanes ridge are much slower [*Gaherty*, 2001]. The velocity variation observed between Ascension, the Azores, and Kolbeinsey are consistent with approximately ±75° potential-temperature variation along axis, while the velocities in Reykjanes lithosphere are difficult to explain using temperature alone. We speculate that the anomalously low shear velocities within the lithosphere produced at the Reykjanes ridge result from ~12% (by volume) gabbro retained in the mantle due to the imbalance between high melt production and inefficient melt extraction along the slow spreading Reykjanes. A similar process could contribute to the (not as) slow velocities along the Kolbeinsey ridge and the MAR near Azores. Radial shear anisotropy in the upper 150 km also indicates an apparent hot spot influence: mantle fabric near Ascension is quite weak, consistent with models of anisotropy produced by corner flow during slow seafloor spreading [*Gaherty et al.*, 2004], while the fabric near the Azores and the Kolbeinsey ridge is larger, suggesting that the hot spot produces temperature and flow conditions that enhance crystallographic alignment beyond that produced by slow seafloor spreading in these regions. None of the regions exhibit the highly anomalous anisotropy found along the Reykjanes.

Acknowledgments

[37] All figures were generated using GMT [*Wessel and Smith*, 1998]. GSN, HOTSPOT, and MIDSEA data were collected from the IRIS Data Management System (http://www.iris.edu). Event parameters were derived from the Global CMT project (http://www.globalcmt.org) [e.g., *Ekström et al.*, 2005]. We thank Saskia Goes and an anonymous referee for useful reviews that helped clarify and improve the paper. This research was supported by NSF grants OCE04-36398 (J. B. G.) and OCE03-37237 (R. A. D.). Lamont-Doherty Earth Observatory contribution 7006.

References

Allen, R. M., et al. (2002), Imaging the mantle beneath Iceland using integrated seismological techniques, *J. Geophys. Res.*, *107*(B12), 2325, doi:10.1029/2001JB000595.

Anderson, D. L. (1989), *Theory of the Earth*, 366 pp., Blackwell Sci., Malden, Mass.

Bijwaard, H., and W. Spakman (1999), Tomographic evidence for a narrow whole mantle plume below Iceland, *Earth Planet. Sci. Lett.*, *166*, 121–126.

Blackman, D. K., and J.-M. Kendall (2002), Seismic anisotropy in the upper mantle 2. Predictions for current plate boundary flow models, *Geochem. Geophys. Geosyst.*, *3*(9), 8602, doi:10.1029/2001GC000247.

Blichert-Toft, J., A. Agranier, M. Andres, R. Kingsley, J.-G. Schilling, and F. Albarède (2005), Geochemical segmentation of the Mid-Atlantic Ridge north of Iceland and ridge–hot spot interaction in the North Atlantic, *Geochem. Geophys. Geosyst.*, *6*, Q01E19, doi:10.1029/2004GC000788.

Brozena, J. M. (1986), Temporal and spatial variability of seafloor spreading processes in the northern South Atlantic, *J. Geophys. Res.*, *91*, 497–510.

Butler, R., et al. (2004), The Global Seismographic Network surpasses its design goal, *Eos Trans. AGU*, *85*, 225–229.

Cannat, M. (1996), How thick is the magmatic crust at slow spreading oceanic ridges?, *J. Geophys. Res.*, *101*, 2847–2857.

Cannat, M., D. Bideau, and H. Bougault (1992), Serpentinized peridotites and gabbros in the Mid-Atlantic Ridge axial valley at 15°37′N and 16°52′N, *Earth Planet. Sci. Lett.*, *109*, 87–106.

Cannat, M., et al. (1999), Mid-Atlantic Ridge–Azores hotspot interactions: Along-axis migration of a hotspot-derived event of enhanced magmatism 10 to 4 Ma ago, *Earth Planet. Sci. Lett.*, *173*, 257–269.

Carlson, R. L., and H. P. Johnson (1994), On modeling the thermal evolution of the oceanic upper mantle: An assessment of the cooling plate model, *J. Geophys. Res.*, *99*, 3201–3214.

Delorey, A. A., R. A. Dunn, and J. B. Gaherty (2007), Surface wave tomography of the upper mantle beneath the Reykjanes Ridge with implications for ridge–hot spot interaction, *J. Geophys. Res.*, doi:10.1029/2006JB004785, in press.

Dosso, L., H. Bougault, C. Langmuir, C. Bollinger, O. Bonnier, and J. Etoubleau (1999), The age and distribution of mantle heterogeneity along the Mid-Atlantic Ridge (31–41°N), *Earth Planet. Sci. Lett.*, *170*, 269–286.

Dunn, R. A., and D. W. Forsyth (2003), Imaging the transition between the region of mantle melt generation and the crustal magma chamber beneath the southern East Pacific Rise with short-period Love waves, *J. Geophys. Res.*, *108*(B7), 2352, doi:10.1029/2002JB002217.

Dunn, R. A., V. Lekić, R. S. Detrick, and D. R. Toomey (2005), Three-dimensional seismic structure of the Mid-Atlantic Ridge (35°N): Evidence for focused melt supply and lower crustal dike injection, *J. Geophys. Res.*, *110*, B09101, doi:10.1029/2004JB003473.

Dziewonski, A. M., and D. L. Anderson (1981), Preliminary reference Earth model, *Phys. Earth Planet. Inter.*, *25*, 297–356.

Ekström, G., A. M. Dziewonski, N. N. Maternovskaya, and M. Nettles (2005), Global seismicity of 2003: Centroid–moment-tensor solutions for 1087 earthquakes, *Phys. Earth Planet. Inter.*, *148*(2–4), 327–351.

Escartin, J., M. Cannat, G. Pouliquen, A. Rabain, and J. Lin (2001), Crustal thickness of V-shaped ridges south of the Azores: Interaction of the Mid-Atlantic Ridge (36–39°N) and the Azores hot spot, *J. Geophys. Res.*, *106*, 21,719–21,735.

Faul, U. H., and I. Jackson (2005), The seismological signature of temperature and grain size variation in the upper mantle, *Earth Planet. Sci. Lett.*, *234*, 119–134.

Foulger, G. R., et al. (2000), The seismic anomaly beneath Iceland extends down to the mantle transition zone and no deeper, *Geophys. J. Int.*, *142*, F1–F5.

Gaherty, J. (2001), Seismic evidence for hotspot-induced buoyant flow beneath the Reykjanes Ridge, *Science*, *293*, 1645–1647.

Gaherty, J. B., T. H. Jordan, and L. S. Gee (1996), Seismic structure of the upper mantle in a central Pacific Corridor, *J. Geophys. Res.*, *101*, 22,291–22,309.

Gaherty, J. B., M. Kato, and T. H. Jordan (1999), Seismological structure of the upper mantle: A regional comparison of seismic layering, *Phys. Earth Planet. Inter.*, *110*, 21–41.

Gaherty, J. B., D. Lizarralde, J. Collins, G. Hirth, and S. Kim (2004), Mantle deformation during slow seafloor spreading constrained by observations of seismic anisotropy in the western Atlantic, *Earth Planet. Sci. Lett.*, *228*, 255–265.

Gee, L. S., and T. H. Jordan (1992), Generalized seismological data functionals, *Geophys. J. Int.*, *111*, 363–390.

Goslin, J., and Triatnord Scientific Party (1999), Extent of Azores plume influence on the Mid-Atlantic Ridge north of the hotspot, *Geology*, *27*, 991–994.

Gu, Y. J., S. C. Webb, A. Lerner-Lam, and J. B. Gaherty (2005), Upper mantle structure beneath the eastern Pacific Ocean ridges, *J. Geophys. Res.*, *110*, B06305, doi:10.1029/2004JB003381.

Hammond, W. C., and E. D. Humphreys (2000), Upper mantle seismic wave velocity: Effects of realistic partial melt geometries, *J. Geophys. Res.*, *105*, 10,975–10,986.

Heller, D.-A., and G. Marquart (2002), An admittance study of the Reykjanes Ridge and elevated plateau between the Charlie-Gibbs and Senja fracture zones, *Geophys. J. Int.*, *148*, 65–76.

Hess, H. H. (1964), Seismic anisotropy of the uppermost mantle under oceans, *Nature*, *203*, 629–630.

Hirth, G., and D. L. Kohlstedt (1996), Water in the oceanic upper mantle: Implications for rheology, melt extraction and the evolution of the lithosphere, *Earth Planet. Sci. Lett.*, *144*, 93–108.

Holtzman, B. K., D. L. Kohlstedt, M. E. Zimmerman, F. Heidelbach, T. Hiraga, and J. Hustoft (2003), Melt segregation and strain partitioning: Implications for seismic anisotropy and mantle flow, *Science*, *301*, 1227–1230.

Hooft, E. E. E., R. S. Detrick, D. R. Toomey, J. A. Collins, and J. Lin (2000), Crustal thickness and structure along three contrasting spreading segments of the Mid-Atlantic Ridge, 33.5°–35°N, *J. Geophys. Res.*, *105*, 8205–8226.

Hooft, E. E. E., B. Brandsdóttir, R. Mjelde, H. Shimamura, and Y. Murai (2006), Asymmetric plume-ridge interaction around Iceland: The Kolbeinsey Ridge Iceland Seismic Experiment, *Geochem. Geophys. Geosyst.*, *7*, Q05015, doi:10.1029/2005GC001123.

Ito, G. (2001), Reykjanes 'V'-shaped ridges originating from a pulsing and dehydrating mantle plume, *Nature*, *411*, 681–684.

Ito, G., J. Lin, and C. W. Gable (1996), Dynamics of mantle flow and melting at a ridge centered hotspot: Iceland and the Mid-Atlantic Ridge, *Earth Planet. Sci. Lett.*, *144*, 53–74.

Ito, G., Y. Shen, G. Hirth, and C. J. Wolfe (1999), Mantle flow, melting, and dehydration of the Iceland mantle plume, *Earth Planet. Sci. Lett.*, *165*, 81–96.

Ito, G., J. Lin, and D. Graham (2003), Observational and theoretical studies of the dynamics of mantle plume–mid-ocean ridge interaction, *Rev. Geophys.*, *41*(4), 1017, doi:10.1029/2002RG000117.

Jackson, I., J. D. Fitz Gerald, U. H. Faul, and B. H. Tan (2002), Grain-size-sensitive seismic wave attenuation in polycrystalline olivine, *J. Geophys. Res.*, *107*(B12), 2360, doi:10.1029/2001JB001225.

Jha, K., E. M. Parmentier, and J. P. Morgan (1994), The role of mantle-depletion and melt-retention buoyancy in spreading-center segmentation, *Earth Planet. Sci. Lett.*, *125*, 221–234.

Jones, S. M., N. White, and J. Maclennan (2002), V-shaped ridges around Iceland: Implications for spatial and temporal patterns of mantle convection, *Geochem. Geophys. Geosyst.*, *3*(10), 1059, doi:10.1029/2002GC000361.

Karato, S. (1993), Importance of anelasticity in the interpretation of seismic tomography, *Geophys. Res. Lett.*, *20*, 1623–1626.

Kelemen, P. B., E. Kikawa, D. J. Miller, and Leg 210 Scientific Party (2004), ODP leg 209 drills into mantle peridotite along the Mid-Atlantic ridge from 14°N to 16°N, *JOIDES J.*, *30*, 14–19.

Kinzler, R. J., and T. L. Grove (1993), Corrections and further discussion of the primary magmas of mid-ocean ridge basalts, 1 and 2, *J. Geophys. Res.*, *98*, 22,339–22,347.

Klein, E. M., and C. H. Langmuir (1987), Global correlations of ridge basalt chemistry with axial depth and crustal thickness, *J. Geophys. Res.*, *92*, 8089–8115.

Klingelhofer, F., T. A. Minshull, D. K. Blackman, P. Harben, and V. Childers (2001), Crustal structure of Ascension Island from wide-angle seismic data: Implications for the formation of near-ridge volcanic islands, *Earth Planet. Sci. Lett.*, *190*, 41–56.

Langmuir, C. H., E. M. Klein, and T. Plank (1993), Petrological systematics of mid-ocean ridge basalts: Constraints on melt generation beneath ocean ridges, in *Mantle Flow and Melt Generation at Mid-ocean Ridges*, *Geophys. Monogr. Ser.*, vol. 71, edited by J. P. Morgan, D. K. Blackman, and J. M. Sinton, pp. 183–281, AGU, Washington, D. C.

Laske, G., G. Masters, and C. Reif (2001), CRUST 2.0, A new global crustal model at 2 × 2 degrees, Univ. of Calif., San Diego, La Jolla. (Available at http://mahi.ucsd.edu/Gabi/rem.html)

Lévêque, J. J., E. Debayle, and V. Maupin (1998), Anisotropy of the Indian Ocean upper mantle from Rayleigh- and Love-waveform inversion, *Geophys. J. Int.*, *133*, 529–540.

Li, A., and R. S. Detrick (2006), Seismic structure of Iceland from Rayleigh wave inversions and geodynamic implications, *Earth Planet. Sci. Lett.*, *241*, 901–912.

Lizarralde, D., J. B. Gaherty, J. A. Collins, G. Hirth, and S. Kim (2004), Spreading-rate dependence of melt extraction at mid-ocean ridges from far-offset seismic data, *Nature*, *432*, 744–747.

Maupin, V. (1985), Partial derivatives of surface wave phase velocities for flat anisotropic models, *Geophys. J. R. Astron. Soc.*, *83*, 379–398.

McKenzie, D., and M. J. Bickle (1988), The volume and composition of melt generated by extension of the lithosphere, *J. Petrol.*, *29*, 625–679.

Minshull, T. A., N. J. Bruguier, and J. M. Brozena (2003), Seismic structure of the Mid-Atlantic Ridge, 8–9°S, *J. Geophys. Res.*, *108*(B11), 2513, doi:10.1029/2002JB002360.

Montagner, J.-P., and J. Ritsema (2001), Interactions between ridges and plumes, *Science*, *294*, 1472–1473.

Montelli, R., G. Nolet, F. A. Dahlen, G. Masters, E. R. Engdahl, and S.-H. Hung (2004), Finite-frequency tomography reveals a variety of plumes in the mantle, *Science*, *303*, 338–343, doi:10.1126/science.1092485.

Mooney, W., G. Laske, and G. Masters (1998), Crust 5.1: A global crustal model at 5 × 5 degrees, *J. Geophys. Res.*, *103*, 727–747.

Mueller, R. D., W. R. Roest, J.-Y. Royer, L. M. Gahagan, and J. G. Sclater (1993), A digital age map of the ocean floor, *SIO Ref. Ser. 93-30*, Scripps Inst. of Oceanogr., La Jolla, Calif.

Nicolas, A., and N. I. Christensen (1987), Formation of anisotropy in upper mantle peridotites: A review, in *Composition, Structure, and Dynamics of Lithosphere-Asthenosphere System*, *Geodyn. Ser.*, vol. 16, edited by K. Fuchs and C. Froidevaux, pp. 111–123, AGU, Washington, D. C.

Nishimura, C. E., and D. W. Forsyth (1988), The anisotropic structure of the upper mantle in the Pacific, *Geophys. J.*, *96*, 203–209.

Parmentier, E. M., and J. Phipps Morgan (1990), Spreading rate dependence of three-dimensional structure in oceanic spreading centers, *Nature*, *348*, 325–328.

Parsons, B., and J. G. Sclater (1977), An analysis of the variation of ocean floor bathymetry and heat flow with age, *J. Geophys. Res.*, *82*, 803–827.

Pilidou, S., K. Priestley, O. Gudmundsson, and E. Debayle (2004), Upper mantle S-wave speed heterogeneity and anisotropy beneath the North Atlantic from regional surface wave tomography: The Iceland and Azores plumes, *Geophys. J. Int.*, *159*, 1057–1076, doi:10.1111/j.1365-246X.2004.02462.x.

Priestley, K., and D. McKenzie (2006), The thermal structure of the lithosphere from shear wave velocities, *Earth Planet. Sci. Lett.*, *244*, 285–301.

Schilling, J. G. (1973), Iceland mantle plume: Geochemical study of Reykjanes Ridge, *Nature*, *242*, 565–571.

Schilling, J.-G., R. Kingsley, D. Fontignie, R. Poreda, and S. Xue (1999), Dispersion of the Jan Mayen and Iceland mantle plumes in the Arctic: A He-Pb-Nd-Sr isotope tracer study of basalts from the Kolbeinsey, Mohns, and Knipovich Ridges, *J. Geophys. Res.*, *104*, 10,543–10,569.

Schutt, D. L., and C. E. Lesher (2006), Effects of melt depletion on the density and seismic velocity of garnet and spinel lherzolite, *J. Geophys. Res.*, *111*, B05401, doi:10.1029/2003JB002950.

Searle, R. C., J. A. Keeton, R. B. Owens, R. S. White, R. Mecklenburgh, B. Parsons, and S. M. Lee (1998), The Reykjanes Ridge: Structure and tectonics of a hot-spot-influenced, slow-spreading ridge, from multibeam bathymetry, gravity, and magnetic investigations, *Earth Planet. Sci. Lett.*, *160*, 463–478.

Sheehan, A. F., and S. C. Solomon (1991), Joint inversion of shear wave travel time residuals and geoid and depth anomalies for long-wavelength variations in upper mantle temperature and composition along the Mid-Atlantic Ridge, *J. Geophys. Res.*, *96*, 19,981–20,009.

Silveira, G., and E. Stutzmann (2002), Anisotropic tomography of the Atlantic Ocean, *Phys. Earth. Planet. Inter.*, *4131*, 1–12.

Smallwood, J. R., R. S. White, and T. A. Minshull (1995), Seafloor spreading in the presence of the Iceland plume: The structure of the Reykjanes Ridge at 61°40′N, *J. Geol. Soc. London*, *152*, 1023–1029.

Smith, W. H. F., and D. T. Sandwell (1997), Global seafloor topography from satellite altimetry and ship depth soundings, *Science*, *277*, 1957–1962.

Stein, C. A., and S. Stein (1992), A model for the global variation in oceanic depth and heat flow with lithospheric age, *Nature*, *359*, 123–129.

Tolstoy, M., A. J. Harding, and J. A. Orcutt (1993), Crustal thickness on the Mid-Atlantic Ridge: Bull's-eye gravity anomalies and focused accretion, *Science*, *262*, 726–729.

Turcotte, D. L., and G. Schubert (2002), *Geodynamics*, Cambridge Univ. Press, New York.

van der Lee, S., et al. (2001), Eurasia-Africa plate boundary region yields new seismographic data, *Eos Trans. AGU*, *82*(51), 637–646.

Vogt, P. R. (1971), Asthenosphere motion recorded by the ocean floor south of Iceland, *Earth Planet. Sci. Lett.*, *13*, 153–160.

Wessel, P., and W. H. F. Smith (1998), New, improved version of the Generic Mapping Tools released, *Eos Trans. AGU*, *79*, 579.

White, R. S. (1997), Rift-plume interaction in the North Atlantic, *Philos. Trans. R. Soc. London, Ser. A*, *355*, 319–339.

White, R. S., J. W. Brown, and J. R. Smallwood (1995), The temperature of the Iceland plume and origin of outward propagating V-shaped ridges, *J. Geol. Soc. London*, *152*, 1039–1045.

White, R. S., T. A. Minshull, M. J. Bickle, and C. J. Robinson (2001), Melt generation at very slow-spreading oceanic ridges: Constraints from geochemical and geophysical data, *J. Petrol.*, *42*, 1171–1196.

Wolfe, C. J., I. T. Bjarnason, J. C. VanDecar, and S. C. Solomon (1997), Seismic structure of the Iceland mantle plume, *Nature*, *385*, 245–247.

Yale, M. M., and J. Phipps Morgan (1998), Asthenosphere flow model of hotspot-ridge interactions: A comparison of Iceland and Kerguelen, *Earth Planet. Sci. Lett.*, *161*, 45–56.